International Journal for Modern Trends in Science and Technology
Volume 11, Issue 09, pages 104-115.
ISSN: 2455-3778 online
Available online at: http://www.ijmtst.com/vol11issue09.html
DOI: https://doi.org/10.5281/zenodo.17171127

A High Gain Extendable Bidirectional DC-DC Converter with Sliding Mode Control for Next-Gen EV Applications

K. Threyini[1] | P. Venkata Narayana[2]

[1]*Department of Electrical and Electronics Engineering, JNTUH University College of Engineering, Science & Technology, Hyderabad, Telangana, India*
[2]*Department of Electrical and Electronics Engineering, JNTUH University College of Engineering, Science &Technology, Hyderabad, Telangana, India*

To Cite this Article
K. Threyini & P. Venkata Narayana (2025). A High Gain Extendable Bidirectional DC-DC Converter with Sliding Mode Control for Next-Gen EV Applications. International Journal for Modern Trends in Science and Technology, 11(09), 104-115. https://doi.org/10.5281/zenodo.17171127

Article Info
Received: 17 August 2025; Accepted: 20 September 2025.; Published: 21 September 2025.

KEYWORDS

SMC,
DC-DC Converter,
Smooth control,
High efficiency,
IOFL,
Electric vehicle

ABSTRACT

This paper focuses on the design and implementation of a Sliding Mode Control (SMC) strategy for an Extendable Bidirectional DC-DC Converter. The SMC approach offers significant advantages such as high robustness against disturbances, fast dynamic response, and excellent stability, which makes it highly suitable for applications involving renewable energy storage systems and electric vehicle power management. Unlike conventional controllers like IOFL, which can suffer from steady-state errors and slower responses, the SMC can efficiently handle non-linearities and abrupt changes in system parameters. The converter is operated in two distinct modes: charge mode and discharge mode. In each mode, the SMC dynamically adjusts the switching states to maintain the desired current and voltage profiles. The theoretical analysis, supported by simulation studies, demonstrates that the proposed controller successfully tracks reference signals with minimal overshoot and reduced settling time. Moreover, the system effectively suppresses the chattering effect commonly associated with SMC by utilizing a boundary layer design, ensuring smoother control action. Through detailed simulation, it is observed that the SMC-based converter achieves higher efficiency and improved performance compared to the conventional IOFL-based system, particularly during rapid load transitions. The results validate that the proposed method provides better control over energy flow, making it an attractive solution for modern energy storage applications.

1. INTRODUCTION

For decades, internal combustion engines (ICEs) have been the backbone of most transportation systems because of their strong reliability. However, in recent years, the steadily increasing prices of diesel and petrol, along with rising environmental concerns and the limited availability of fossil fuels, have pushed major automobile companies to search for better and more sustainable fuel alternatives that can meet both performance and reliability demands. The transportation sector is, in fact, one of the largest sources of pollution worldwide, significantly contributing to greenhouse gas emissions. According to the Union of Concerned Scientists in the United States, nearly 30% of global greenhouse gas emissions come from vehicle use. In hybrid electric vehicles (HEVs), an electric motor is responsible for driving the vehicle, while the internal combustion engine supports the system by charging the batteries and providing additional power through a converter system. Typically, an HEV consists of a rectifier to convert the AC voltage from the generator into DC, a DC-DC converter to manage the charging and discharging of the battery, and an inverter to convert the DC voltage into AC, making it suitable for the motor's operation. HEVs are generally known for their durability and lower maintenance needs. Batteries play a crucial role in electric vehicles (EVs), but they typically provide low DC voltages such as 12V, 24V, or 48V. To power electric motors, this voltage must be stepped up to a higher level using a DC-DC converter, which can also work in the reverse direction when required.

When designing DC-DC converters for EVs, key considerations include voltage conversion capability, energy efficiency, electromagnetic interference (EMI) control, power density, and bidirectional power flow. Although high voltage gains can be achieved using coupled inductors or transformers, these designs often lead to bulkier systems with lower efficiency and problems like leakage inductance. To minimize EMI, common-ground converter configurations are preferred. Importantly, the DC-DC converter must allow energy to flow both from the battery to the motor and back from the motor to the battery to ensure optimal system operation. The limitation of unidirectional power flow in conventional converters restricts their suitability for electric vehicle (EV) applications. To overcome this issue, a bidirectional DC-DC converter with high voltage gain is essential to satisfy the operational demands of EV systems.

In response to this need, this paper introduces a bidirectional, non-isolated, common-ground, high-gain DC-DC converter specifically designed for EV applications. In the proposed design, the low-voltage (LV) side is directly connected to the EV's battery, while the high-voltage (HV) side supplies power to the electric motor. During discharge operation, the motor draws energy from the battery, causing current to flow from the LV side to the HV side. In contrast, during the charging process, this current direction is reversed to recharge the battery through the HV side. The converter structure combines a high-gain quadratic boost converter and two buck converters arranged in cascade. Some key components, such as inductors, capacitors, switches, and diodes, are strategically shared among these converter stages, which helps to build an efficient bidirectional system. Thanks to this shared design, the converter can be scaled to achieve a significant voltage increase during both charging a discharging cycles.

A mathematical model of the proposed converter is developed, and based on this, a nonlinear control strategy is implemented to manage the voltage and current in both operational modes. The controller is designed using boundary conditions depending on the desired output which is known as Sliding mode controller (SMC).

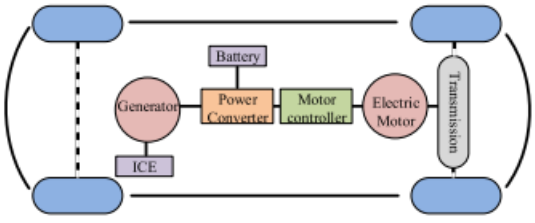

Fig. 1. Schematic of electromotive force of an HEV

2. MODELING AND ANALYSIS OF PROPOSED CONVERTER

The proposed extendable high-gain bidirectional DC-DC converter is developed by combining a quadratic boost converter, as referenced in [18], and a quadratic buck converter. The quadratic buck stage is designed

using two conventional buck converters connected in series, as described in [19]. Figures 2(a) and 2(b) present the individual configurations of the quadratic boost and quadratic buck converters, respectively. The complete structure of the proposed DC-DC converter, which integrates both the quadratic boost and buck converters, is illustrated in Figure 2(c)

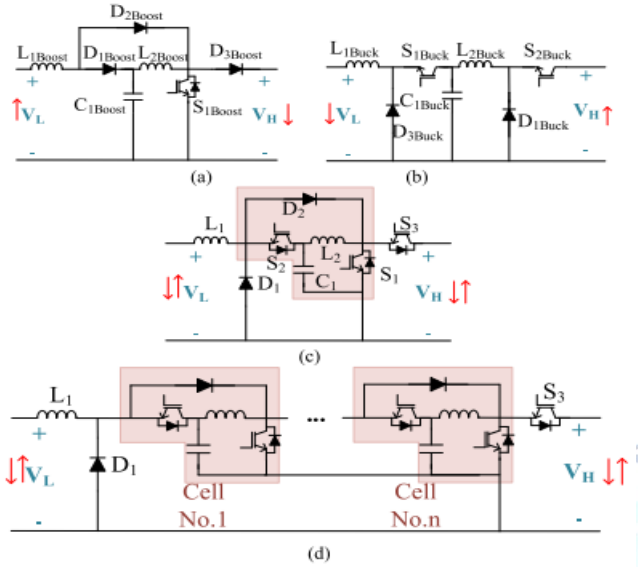

Fig. 2. Configuration of the proposed converter and its contents. (a) Fundamental quadratic boost converter [18]. (b) Cascaded buck converter [19]. (c) Proposed quadratic bidirectional DC–DC converter. (d) Extended configuration of the proposed converter

One of the key features of this converter is its common-ground design between the input and output terminals, and its non-isolated nature. By eliminating isolation, this converter addresses common drawbacks found in isolated converter systems, such as leakage inductance and high voltage stress across semiconductor components. Additionally, by expanding the design into n-cell configurations, as shown in Figure 2(d), the converter can achieve high voltage gains. This approach offers the benefits of high voltage gain similar to isolated converters while avoiding the typical challenges those systems face. Figure 3 provides a detailed view of the proposed bidirectional DC-DC converter with a single cell, which consists of three switching devices, two diodes, two inductors, and two capacitors. This converter is capable of operating in both charging and discharging modes. The operational principles of these modes, along with the corresponding mathematical modelling and analysis, are discussed in the following subsections

A. Discharge mode

The operating states during the discharging (boost) mode are illustrated in Figures 4(a) and 4(b). According to these diagrams, the converter operates in two distinct states when discharging, and the switching configurations for the switches and diodes in each state are summarized in Table I.

One of the key features of this converter is its common-ground design between the input and output terminals, and its non-isolated nature. By eliminating isolation, this converter addresses common drawbacks found in isolated converter systems, such as leakage inductance and high voltage stress across semiconductor components. Additionally, by expanding the design into n-cell configurations, as shown in Figure 2(d), the converter can achieve high voltage gains. This approach offers the benefits of high voltage gain similar to isolated converters while avoiding the typical challenges those systems face. Figure 3 provides a detailed view of the proposed bidirectional DC-DC converter with a single cell, which consists of three switching devices, two diodes, two inductors, and two capacitors. This converter is capable of operating in both charging and discharging modes. The operational principles of these modes, along with the corresponding mathematical modelling and analysis, are discussed in the following subsections

Fig. 2. Configuration of the proposed converter and its contents. (a) Fundamental quadratic boost converter [18]. (b) Cascaded buck converter [19].(c) Proposed quadratic bidirectional DC–DC converter. (d) Extended configuration of the proposed converter.

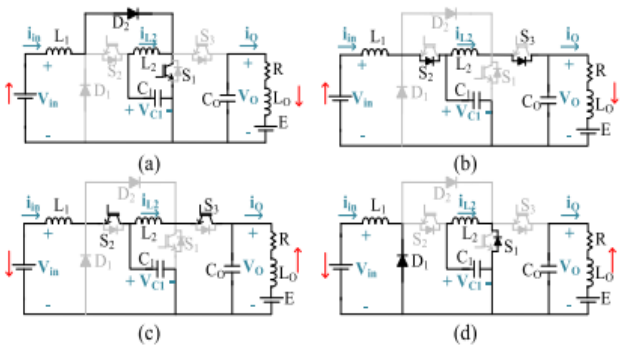

Fig. 4. Operating states of (a) discharge mode (state I), (b) discharge mode(state II), (c) charge mode (state I), and (d) charge mode (state II).

Figure 5(a) presents the voltage and current waveforms associated with the switches and diodes across different switching states. As depicted, the switching cycle spans a period T = 1/fs, beginning at t_0 and ending at t_2. The duty cycle of switch S1 is denoted as d_1. In the same figure, g_1, g_2, and g_3 represent the gate signals for switches S1, S2, and S3, respectively. Likewise, i_{s1}, i_{s2}, i_{s3}, iD_1, and iD_2 denote the current through the switches and diodes. The energy flow among the circuit components during discharging mode can be explained in stages:

First State (from t_0 to t_1): As illustrated in Figures 4(a) and 5(a), inductor L1 stores energy directly from the input voltage Vin, while inductor L2 is charged via capacitor C1. Meanwhile, the load continues to receive power through the output capacitor Co.

Table1: switching states of discharge mode

States	*Duration time*	*Switches/Diodes state*				
		S1	*S2*	*S3*	*D1*	*D2*
1	$\boldsymbol{d_1T}$	*On*	*Off*	*Off*	*Off*	*On*
2	$\boldsymbol{(1-d_1)T}$	*Off*	*On*	*On*	*Off*	*Off*

Second state (from t1 to t2): As shown in Figs. 4(b) and 5(a), C1 is charged through L1, and L2 both charges Co and provides the output current.

To design a robust controller, accurate modelling of the converter is essential. The system can be represented by a set of state-space differential equations derived using Kirchhoff's voltage and current laws.

Let:

- $x_1 = i_{L1}$ (inductor L1 current)
- $x_2 = i_{L2}$ (inductor L2 current)
- $x_3 = V_{C1}$ (voltage of intermediate capacitor C1)
- $x_4 = V_{C2}$ (voltage of intermediate capacitor C2)
- $x_5 = V_O$ (output voltage)

In this mode, the power flows in the expected direction: from the input source to the load. The input voltage pushes current through the inductors and capacitors, eventually delivering energy to the load.

During the ON and OFF switching states:

• ON state: L1 and L2 are charged

• OFF state: Energy is transferred from inductors through C1 and C2 to the output

Where the state-space variables (x) and the input vector (u) are defined as

$$x = \begin{bmatrix} i_{in} \\ i_{L2} \\ V_{C1} \\ V_O \\ i_O \end{bmatrix}, u = \begin{bmatrix} V_{in} \\ E \end{bmatrix}. \quad (1)$$

Using averaged modelling:

$$\frac{dx_1}{dt} = \frac{1}{L_1}(V_{in} - V_{C1})$$

Inductor L1 pulls current from the input source and transfers energy to Capacitor C1.

$$\frac{dx_2}{dt} = \frac{1}{L_2}(V_{C1} - V_{C2})$$

Inductor L2 helps move energy from Capacitor C1 to Capacitor C2 and towards the load.

$$\frac{dx_3}{dt} = \frac{1}{C_1}(i_{L1} - i_{L2})$$

Capacitor C1 acts as a middle energy storage, temporarily holding the charge.

$$\frac{dx_4}{dt} = \frac{1}{C_2}(i_{L2} - i_{Load})$$

Capacitor C2 smooths out the voltage supplied to the load, reducing ripples.

Neglecting losses (ideal condition) and considering different battery-side voltage values. In the extended converter with n cells, the relation between Vin and VO is as follows:

$$M_{boost} = \frac{V_O}{V_{in}} = \frac{1}{(1-d_1)^{n+1}}$$

Where M_{boost} is the voltage gain in boost (discharging) mode.

It is obvious that, given a certain $d1$, the voltage gain raises in line with increasing the number of cells (n).

B. Charge mode

The charging (buck) mode is shown in Fig. 4(c) and (d). As shown, this mode consists of two different states, and the switching conditions for the switches and diodes in each state are detailed in Table II. The corresponding voltages and currents across the switches and diodes for these operational states are presented in Fig. 5(b)

Table 2: switching states of charge mode

States	*Duration time*	*Switches/Diodes state*				
		S1	*S2*	*S3*	*D1*	*D2*
1	$\boldsymbol{d_3T}$	*Off*	*On*	*On*	*Off*	*Off*
2	$\boldsymbol{(1-d_3)T}$	*On*	*Off*	*Off*	*On*	*Off*

As illustrated in the figure, the switching period is defined as T=1/fsT = 1/fsT=1/fs , and the duty cycle associated with switches S3 and S4 is denoted as d3d_3d3. In this figure, g1g_1g1, g2g_2g2, and g3g_3g3 represent the gate signals for switches S1, S2, and S3 respectively, while iS1,iS2,iS3,iD1, and iD2 indicate the currents flowing through the switches and diodes.

The energy transfer process within the circuit components during charging mode can be summarized as follows:

First State (from t_0 to t_1): As depicted in Figs. 4(c) and

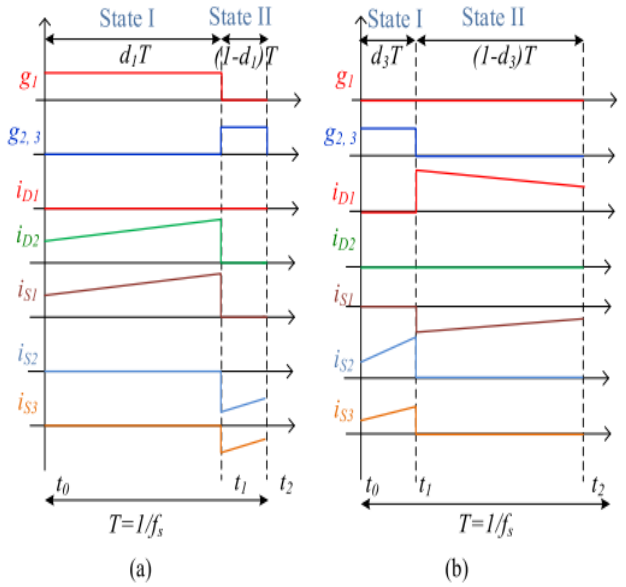

5(b), capacitor C1 is charged via inductor L2 and capacitor Co, while inductor L1 is charged through C1C_1C1. Additionally, the input voltage source Vin supplies current through L1.

Second state (from t1 to t2) As shown in Figs. 4(d) and 5(b), the remaining current in inductor L2 continues to charge capacitor C1, and the residual current in L1 flows back to the input source via diode D1.

Fig. 5. Waveforms and switching states in (a) discharge mode and (b) charge mode.

In this mode, the direction of energy flow is reversed. Power flows from the load back towards the source. This is useful in systems where energy recovery is needed, such as electric vehicles during braking (regenerative braking).

In buck mode, the equations are modified to represent reverse energy flow:

$$\frac{dx_1}{dt} = \frac{1}{L_1}(V_{C1} - V_{in})$$

Inductor L1 now transfers energy back to the input side, reducing the input's net power consumption.

$$\frac{dx_2}{dt} = \frac{1}{L_2}(V_{C2} - V_{C1})$$

Inductor L2 pushes energy from the output side (Capacitor C2) towards Capacitor C1.

$$\frac{dx_3}{dt} = \frac{1}{C_1}(i_{L2} - i_{L1})$$

Capacitor C1 and **Capacitor C2** still manage the energy storage but now support reverse power flow

$$\frac{dx_4}{dt} = \frac{1}{C_2}(i_{LOAD} - i_{L2})$$

Even though the load still consumes power, part of the energy is now recovered and sent back to the source. charge mode allows the converter to recover unused or excess energy and recycle it into the system.

$$M_{buck} = \frac{V_{in}}{V_O} = (d_3)^{n+1}$$

Where M_{buck} is the voltage gain in buck (charging) mode. It is obvious that, given a certain $d3$, the voltage gains decrease in line with the number of cells (n).

3. NONLINEAR CONTROL OF PROPOSED CONVERTER WITH SLIDING MODE CONTROLLER

Sliding Mode Control (SMC) is a robust, nonlinear control technique that forces system trajectories to "slide" along a predefined surface to achieve the desired system behaviour. The sliding surface is carefully designed to ensure system stability and fast error convergence.

1) Sliding Surface Design

The sliding surface is the core of SMC. It defines the condition that system states must satisfy to achieve robust performance. For voltage tracking, the sliding surface is formulated using the output voltage tracking error and its derivative.

$$S(t) = \dot{e}(t) + \lambda e(t)$$

2) Stability and Lyapunov Function

The Lyapunov function is used to confirm the global stability of the SMC-controlled system. The Lyapunov candidate function is the square of the sliding surface. Its derivative must be negative definite to ensure the system states reach and remain on the sliding surface.

$$V(S) = \frac{1}{2}S^2$$

The time derivative of the Lyapunov function must satisfy the sliding condition, which is defined by the reaching law.

$$\dot{V}(S) = S\dot{S} = -\eta|S|$$

3) Chattering and Boundary Layer

Chattering is a typical problem in SMC caused by high-frequency switching. To mitigate this, a boundary layer is introduced by replacing the discontinuous sign function with a continuous saturation function.

$$Sat\left(\frac{S}{\phi}\right) = \begin{cases} 1 & S > \phi \\ S/\phi & |S| \le \phi \\ -1 & S < -\phi \end{cases}$$

4) Practical Controller Parameter Selection

Parameter	Purpose
λ	Controls the speed of error convergence
η	Provides sufficient switching gain
ϕ	Reduces chattering via boundary layer

A.SMC Design for Discharge Mode (Boost Mode)

1) Control Objective:

The primary goal in discharge mode is to regulate the output voltage VOV_O such that it accurately tracks a desired reference voltage Vo to track Vo ref even in the presence of load disturbances and parameter variations. The Sliding Mode Controller ensures that the system trajectory is always driven towards the desired output voltage and rejects disturbances robustly.

2) Detailed Dynamics:

The output voltage dynamics of the converter are primarily governed by the relationship between the output inductor current and the load current . According to the converter model, the rate of change of the output voltage is influenced by the difference between these two currents, scaled by the output capacitance.

$$\dot{V_O} = \frac{i_{L2} - i_O}{C_O}$$

The output inductor current iL2 can be further expanded to include the dependency on the duty cycle d1d_1 and the intermediate capacitor voltage VC1. The inductor current is affected by the voltage applied across it and the energy stored in the inductor. Using the voltage-second balance, the following expression is derived:

$$i_{L2} = \frac{L_2.i_{L2} + V_O}{D_1.V_{C1}}$$

This equation links the inductor current directly to the system states and the control input, which is crucial for SMC design as the controller must actively adjust d1d_1 to track the output voltage.

3) Sliding Surface:

The sliding surface is a critical part of the SMC design. It is selected to ensure that the system error converges to zero rapidly. In this case, the sliding surface is defined based on the rate of change of the output voltage and the voltage tracking error. The proportional-derivative structure of the sliding surface guarantees both fast transient response and minimal steady-state error.

$$S(t) = \dot{V_O} + \lambda(V_O - V_{Oref})$$

Here, λ lambda is a positive constant that determines how aggressively the controller responds to deviations from the reference voltage.

4) Reaching Law:

To ensure that the system states are consistently attracted towards the sliding surface, a reaching law is enforced. The reaching law dictates how the sliding variable s(t)s(t) should evolve over time to satisfy the sliding condition. It is carefully chosen to provide finite-time convergence and disturbance rejection.

$$\dot{S}(t) = -\eta.Sat(\tfrac{S}{\phi})$$

The parameter η represents the switching gain that must be selected to dominate model uncertainties and external disturbances, while ϕ\phi defines the boundary layer to reduce chattering.

5) Control Law:

The equivalent control duty cycle deq is the ideal control input that would maintain the system on the sliding surface in the absence of disturbances. It is derived by setting the sliding surface to zero and solving for the control input. This provides a feedforward component that stabilizes the system.

$$d_{eq} = \frac{fV_O(x) + \lambda(V_O - V_{Oref})}{gV_O(x)}$$

The final control law includes the switching term, which compensates for modelling errors and ensures robust tracking performance. This complete control law is implemented to regulate the duty cycle in discharge mode.

$$d_1 = d_{eq} - \frac{\eta.Sat(S/\phi)}{gV_O(x)}$$

This law effectively drives the system to the sliding

surface and maintains it there, guaranteeing voltage regulation despite parameter uncertainties.

B. SMC Design for Charge Mode (Buck Mode)

1) Control Objective:

In charge mode, the primary objective is to regulate the input current iin to track a reference current Iin ref. This ensures that the battery charging process is properly controlled and the converter operates efficiently and safely

2) Detailed Dynamics:

The input current dynamics are derived from the input inductor equation. The rate of change of the input current is influenced by the difference between the input voltage Vin and the intermediate capacitor voltage VC1, scaled by the input inductance L1.

$$\dot{\iota_{in}} = \frac{V_{in} - V_{C1}}{L_1}$$

This expression is central to the design of the sliding surface and control law because it directly relates the control input to the desired tracking current.

3) Sliding Surface:

The sliding surface for charge mode is formulated to minimize the tracking error of the input current. By including both the derivative of the input current and the tracking error, the surface ensures a rapid and stable response.

$$S(t) = \dot{\iota_{in}} + \lambda(i_{in} - i_{in\,ref})$$

Here, the parameter λ controls the speed of convergence and the responsiveness of the controller.

4) Reaching Law:

The reaching law is applied to ensure the system's trajectory is consistently driven towards the sliding surface. This law introduces the switching control effort necessary to reject disturbances and model uncertainties.

$$\dot{S}(t) = -\eta . Sat(\frac{S}{\phi})$$

The reaching gain η must be sufficiently large to guarantee convergence even in the presence of uncertainties, while the boundary layer parameter ϕ limits chattering.

5) Control Law:

The equivalent duty cycle deq is calculated based on the system dynamics and the sliding surface definition. It represents the nominal duty cycle required to keep the system on the sliding surface.

$$d_{eq} = \frac{f i_{in}(x) + \lambda(i_{in} - i_{in\,ref})}{g i_{in}(x)}$$

To ensure robustness against parameter variations and disturbances, the final control law for charge mode includes the discontinuous switching term.

$$d_3 = d_{eq} - \frac{\eta . Sat(S/\phi)}{g i_{in}(x)}$$

This duty cycle is actively controlled by the SMC to maintain precise input current regulation throughout the charging process

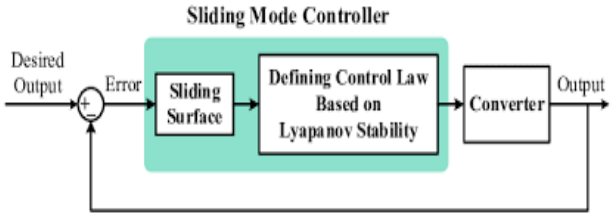

Fig.6. Block diagram of SMC

4. SMC V/S IOFL

Detailed Comparison Between IOFL and SMC Controllers

The comparison in all kind of aspects is observed in Table3,Table 4,Table 5, Table 6.

1) Theoretical Comparison

Feature	IOFL Controller	SMC Controller
Core Concept	Feedback linearization using full converter model	Nonlinear sliding mode based on reaching law
Stability Guarantee	Model-dependent (requires accurate parameters)	Lyapunov-based global stability (model-independent)
Robustness	Poor under parameter variation and load changes	Strong robustness to disturbances and uncertainties
Control Law	Derived from system inversion	Derived from sliding surface dynamics
Chattering	None	Present (reduced via boundary layer design)

2) Mathematical Modelling Comparison

IOFL Controller:

Requires full nonlinear state-space model, must linearize around each operating point, Sensitive to model mismatches.

Control Law Example:

$$u = -f(x) + v$$

Where:

- f(x) is the system nonlinear function.
- v is the new linearized input.

SMC Controller:

Requires dominant system dynamics only, sliding surface designed based on error dynamics, Control law is derived via reaching law and Lyapunov stability.

Sliding Surface:

$$S(t) = \dot{e}(t) + \lambda e(t)$$

Control Law:

$$d = d_{eq} - \frac{\eta . Sat(S/\phi)}{g(x)}$$

SMC is much simpler to design and less dependent on exact system modelling.

3) Converter Interaction Comparison

Feature	IOFL Controller	SMC Controller
Load Variation Sensitivity	High	Low
Input Voltage Fluctuation Tolerance	Poor	Strong
Mode Switching Robustness	Weak	Excellent
Response to Uncertainties	Sensitive	Invariant on sliding surface

4)Implementation Complexity

Parameter	IOFL Controller	SMC Controller
Real-Time Computation	Medium to High	Low
Controller Gains	Complex matrices	Simple gains
Sensor Requirements	All system states	Selected key states (error and derivatives)
Coding Effort	Medium	Low

5) Performance Comparison (Graphical Concept)

Response Time Graph

Response Type	IOFL Controller	SMC Controller
Speed	Moderate	Fast
Overshoot	Possible	Minimal
Steady-State Error	Small (if model perfect)	Very small (even with uncertainties)

IOFL Response: Slower, possible overshoot.

SMC Response: Faster, robust, no overshoot

6) Ripple and Chattering Comparison

.Parameter	IOFL Controller	SMC Controller
Output Ripple	Moderate	Lower
Input Ripple	Moderate	Lower
Chattering	None	Present but controlled using boundary layer

Chattering Control in SMC

Chattering is mitigated using:

$$Sat\left(\frac{S}{\phi}\right) = \begin{cases} 1 & S > \phi \\ S/\phi & |S| \le \phi \\ -1 & S < -\phi \end{cases}$$

The boundary layer width ϕ balances:

- Smaller ϕ: Better accuracy, more chattering.

Larger ϕ: Less chattering, small steady-state error.

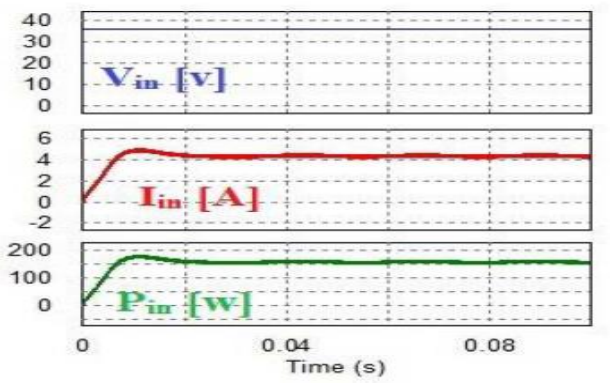

(a)

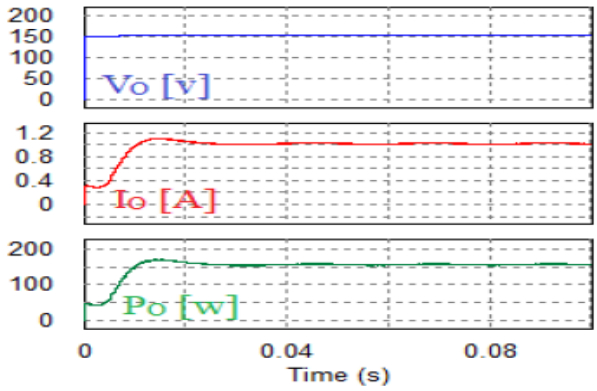

(b)

Fig 7. a) Simulation and experimental results of input voltage, current, and instantaneous active power in discharge (boost) mode. b)Simulation and experimental results of output voltage, current and power.

IOFL is model-driven and precise but is fragile to changes in system parameters. SMC is robust and maintains excellent performance even with parameter uncertainties and mode changes., SMC is easier to tune and implement in real-time systems (e.g., EVs, battery chargers).The fig 7 and fig 8 shows input and output of

converter with IOFL uses large capacitance and inductance value which tends to increase in losses and reduce the efficiency. While in SMC the component sizing is much less comparing to the IOFL equipped converter. Chattering can be minimized by different methods while converter is equipped with sliding mode controller.

5. SIMULATION VERIFICATION

In this simulation, the converter is modelled with its standard equations, considering both the inductor current and capacitor voltage as key state variables. The SMC controller is applied to regulate these states within desired limits during the discharge process. The simulation includes varying load conditions to test the controller's ability to maintain stable output despite sudden changes.

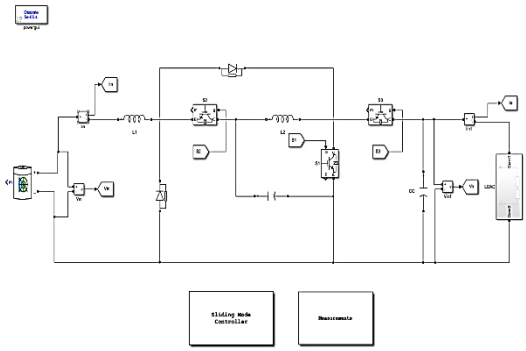

Fig 8. Simulation of extendable bidirectional converter with SMC controller

The discharge mode typically involves reducing the input current while maintaining energy flow to the load. The SMC responds to the real-time system error by switching the converter's switches at high speed, generating the appropriate duty

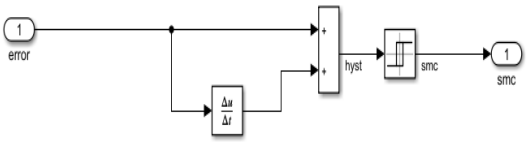

Fig 9. Error calculating loop of SMC

cycle to control energy transfer. This fast switching ensures that the system quickly settles to the desired output after any disturbance.

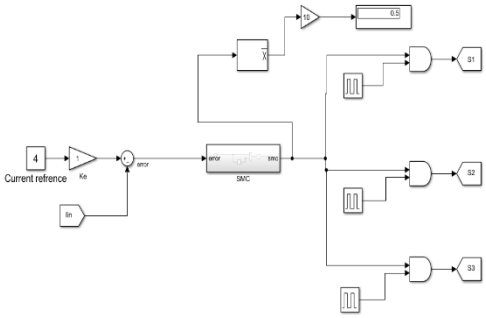

Fig 10. Simulation of SMC control loop

Overall, the simulation of the converter in discharge mode with SMC highlights the controller's ability to provide strong dynamic performance, fast settling time, and minimal steady-state error. By accurately following the sliding surface, the SMC ensures that the system efficiently manages energy delivery to the load, even in the presence of uncertainties and load changes

In the simulation of the converter under charge mode, the system is modelled using its fundamental state-space equations, typically involving inductor current and capacitor voltage as key variables. The SMC controller is designed to generate appropriate switching signals based on the system's real-time state, ensuring the converter can quickly adapt to changes and maintain stable charging behaviour.

During charging, the system demands a controlled increase in the input current. The SMC responds dynamically by adjusting the duty cycle in real-time, ensuring the input current follows the reference smoothly, even under sudden load variations or system disturbances. The fast switching nature of SMC allows the system to respond quickly to these changes, minimizing overshoot and reducing the time required to reach the steady-state

The simulation tests the SMC controller under different charging scenarios, including variations in input voltage and load conditions, to verify the robustness of the controller. The results demonstrate that SMC can effectively regulate the charging process, delivering fast settling times, low steady-state error, and strong resilience against disturbances.

Where $\Delta VC1$, $\Delta VC2$ and Δiin, $\Delta iL2$ are capacitors voltage and inductances current ripples, respectively. Inductances value with respect to their current's ripples and d ($d1$ or $d3$) . It is obvious that decreasing in current ripple necessitates using large inductance. Capacitors

values variation with respect to their voltage ripples and d ($d1$ or $d3$) .It is evident that decreasing in voltage ripple value necessitates using capacitor. d is $d1$ and $d3$ in discharge and charge modes, respectively.

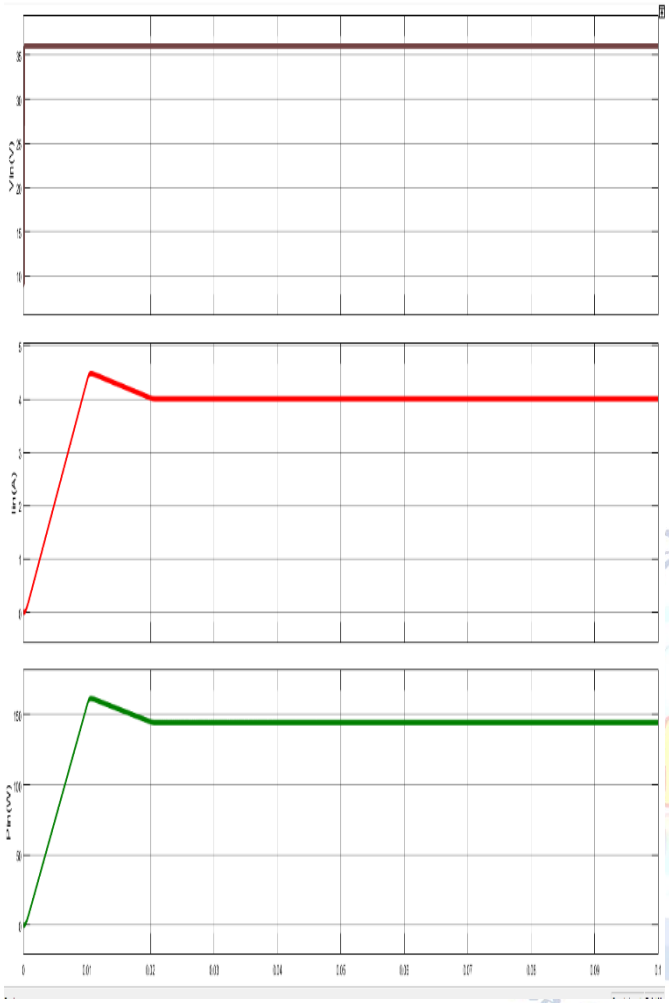

Fig 11. Simulation input of voltage, current and power of converter in boost mode

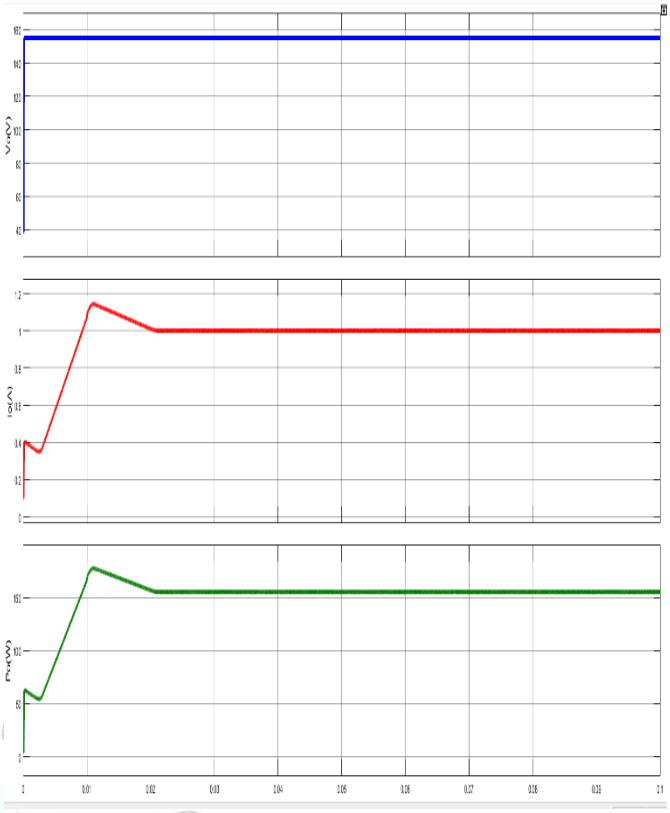

Fig 12. Simulation output of voltage, current and power of converter in buck mode

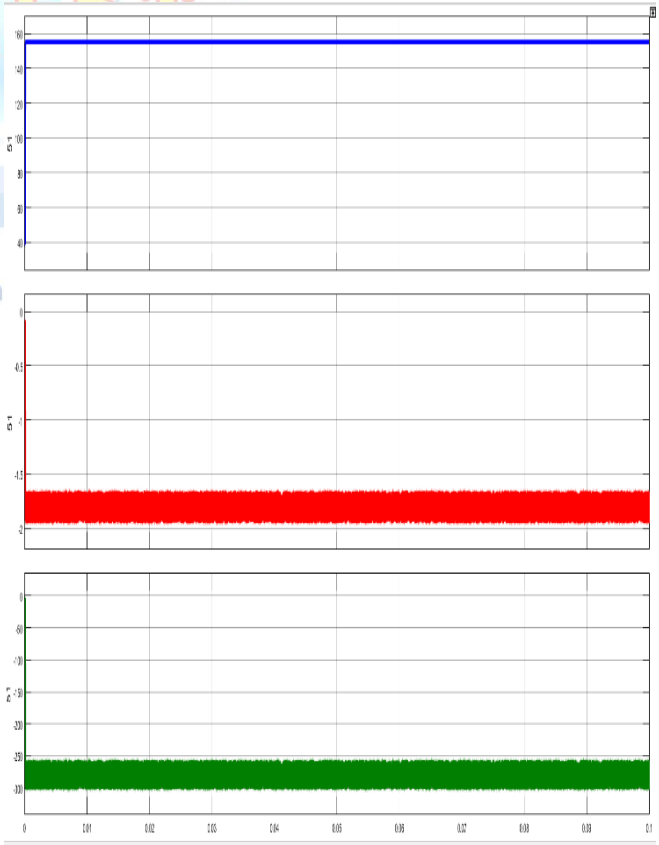

Fig 13. . Simulation output of voltage, current and power of converter in boost mode

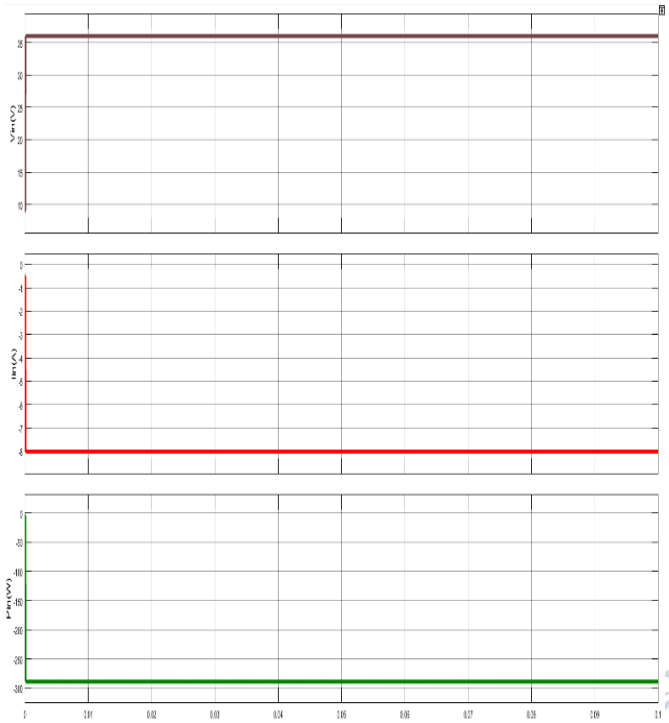

Fig 14. Simulation input of voltage, current and power of converter in buck mode

6. CONCLUSION

Sliding Mode Control (SMC) and Input Output Feedback Linearization (IOFL). The primary aim was to understand which control approach delivers better performance when the system is subjected to sudden load changes and parameter variations. The study was carried out through system modelling, simulation, and detailed analysis of the control responses.

Throughout the work, the Sliding Mode Control method demonstrated significant advantages in handling system disturbances and uncertainties. It consistently provided fast response times and showed strong capability in maintaining system stability, even when the system parameters deviated from their normal values. SMC's ability to drive the system toward a predefined sliding surface and keep it there proved to be highly beneficial. This feature makes it a strong candidate for practical applications where the working environment is not always predictable or ideal.

In contrast, the Input Output Feedback Linearization method provided smoother and more continuous control actions with less aggressive switching. Under ideal and steady operating conditions, IOFL worked quite well and showed a reduction in the high-frequency switching problem often seen in SMC. However, IOFL's major limitation is its sensitivity to changes in system parameters. When the system faced unexpected disturbances or when there was a slight mismatch between the actual system and its mathematical model, the performance of IOFL dropped noticeably. This makes IOFL more suitable for systems where exact parameter knowledge is available and the working environment remains stable.

The simulation results throughout this study clearly supported these observations. In both charging and discharging operations, SMC showed better results by providing faster settling times, smaller steady-state errors, and more reliable control during disturbances. It also managed switching logic and duty cycle variations efficiently, which is crucial in ensuring the desired operation of power electronic circuits.

However, it is important to note that SMC is not without its drawbacks. The rapid switching behaviour, often called chattering, is a known issue that can put extra strain on switching devices and potentially reduce their lifespan. Although IOFL offers smoother control and helps reduce such switching problems, it does not perform well when the system experiences parameter variations or sudden load changes. This shows a natural trade-off between control stability and control smoothness.

Based on the results and observations from this study, it can be concluded that SMC is better suited for systems that require quick responses and strong robustness against disturbances. While its chattering effect needs to be carefully managed, it offers a more dependable solution compared to IOFL, especially in situations where real-world uncertainties are present. Future studies may focus on advanced SMC designs or combined control strategies to reduce chattering while preserving the benefits of robust control.

Conflict of interest statement

Authors declare that they do not have any conflict of interest.

REFERENCES

[1] H.Aouzellag,K. Ghedamsi, and D. Aouzellag, "Energy management and fault tolerant control strategies for fuel cell/ultra-capacitor hybrid electric vehicles to enhance autonomy,

efficiency and life time of the fuel cell system," Int. J. Hydrogen Energy, vol. 40, no. 22, pp. 7204–7213, 2015.

[2] A. R. Gopal, W. Y. Park, M. Witt, and A. Phadke, "Hybrid-and battery electric vehicles offer low-cost climate benefits in China," Transp. Res. Part D: Transp. Environ., vol. 62, pp. 362–371, 2018.

[3] K. J. Reddy and S. Natarajan, "Energy sources and multi-input DC-DC converters used in hybrid electric vehicle applications–A review," Int. J. Hydrogen Energy, vol. 43, no. 36, pp. 17387–17408, 2018.

[4] S. H. Hosseini, F. Sedaghati, and M. Sarhangzadeh, "Modelling and simulation of a new single phase ac-ac converter," in Proc. Int. Conf. Elect. Electron. Eng.-ELECO, 2009, pp. I–226–I–229

[5] S. Salehahari, E. Babaei, and M. Sarhangzadeh, "A hybrid coupled inductor 9-level inverter," in Proc. 29th ITC-CSCC Conf., 2014, pp. 38–41.

[6] S. Salehahari, E. Babaei, and M. Sarhangzadeh, "A new structure of multilevel inverters based on coupled inductors to increase the output current," in Proc. 6th Power Electron., Drive Syst. Technol. Conf., 2015, pp. 19–24.

[7] T. L. Skvarenina, The Power Electronics Handbook. Boca Raton, FL, USA: CRC Press, 2018.

[8] Y. Mei, Q. Jiang, H. Yang, W. Li, X. He, and S. Li, "Non-isolated stacked bidirectional soft-switching DC-DC converter with PWM plus phase-shift control scheme," J. Modern Power Syst. Clean Energy, vol. 5, no. 4, pp. 631–641, 2017.

[9] N. Elsayad, H. Moradisizkoohi, and O. A. Mohammed, "A new hybrid structure of a bidirectional DC-DC converter with high conversion ratios for electric vehicles," IEEE Trans. Veh. Technol., vol. 69, no. 1, pp. 194–206, Jan. 2020.

[10] S. H. Hosseini, R. Ghazi, and H. Heydari-Doostabad, "An extendable quadratic bidirectional DC–DC converter for V2G and G2V applications," IEEE Trans. Ind. Electron., vol. 68, no. 6, pp. 4859–4869, Jun. 2021.

[11] H. Moradisizkoohi, N. Elsayad, and O. A. Mohammed, "A voltage quadrupler interleaved bidirectional DC–DC converter with intrinsic equal current sharing characteristic for electric vehicles," IEEE Trans. Ind. Electron., vol. 68, no. 2, pp. 1803–1813, Feb. 2021.

[12] A. Sharma, S. S. Nag, G. Bhuvaneswari, and M. Veerachary, "Analysis and transition techniques for a bidirectional DC–DC converter," IEEE J. Emerg. Sel. Topics Power Electron., vol. 9, no. 2, pp. 1428–1443, Apr 2021.

[13] H.Heydari-doostabad and T. O'Donnell, "A wide-range high-voltage-gain bidirectional DC–DC converter for V2G and G2V hybrid EV charger," IEEE Trans. Ind. Electron., vol. 69, no. 5, pp. 4718–4729, May 2022 .

[14] V. F. Pires, D. Foito, and A. Cordeiro, "A DC–DC converter with quadratic gain and bidirectional capability for batteries/supercapacitors," IEEE Trans. Ind. Appl., vol. 54, no. 1, pp. 274–285, Jan./Feb. 2018.